

## Supporting Information

### Microfluidic separation of pancreatic islets from exocrine acinar tissue for transplant applications

Walter B. Varhue<sup>a</sup>, Linda Langman<sup>c</sup>, Molly Kelly-Goss<sup>b</sup>, Morgan Lataillade<sup>b</sup>, Kenneth L. Brayman<sup>c</sup>, Shayn Peirce-Cottler<sup>b</sup>, Nathan S. Swami<sup>\*,a</sup>

a – Department of Electrical & Computer Engineering, University of Virginia, Charlottesville, Virginia-22904, USA

b – Department of Biomedical Engineering, University of Virginia, Charlottesville, VA 22904.

c – Department of Surgery, School of Medicine, University of Virginia, Charlottesville, VA 22904

#### **S1: Justification of design criteria used for the multichannel continuous separation device:**

Description of how threshold bypass pressures from the single channel batch mode device (Fig. 1 of manuscript) is used to design a multichannel continuous flow separation device (Fig. 2) by adjusting the deformation pressure and channel width for enabling facile acinar deformation versus that of islets.

#### **S2: Calculation of volumetric flowrate through threshold bypass pressure measurement device:**

Description and results from the hydraulic circuit model used to compute volumetric flowrate through the single channel batch mode device for a range of experimentally measured applied pressures, so that these volumetric flowrates can be used to determine the flowrates for running the separation device.

**S3: Minimizing flowrate differences across the separation device footprint for a number of bifurcating channels:** In this section, we outline the design parameters used to optimize the separation device design to avoid significant variation in volumetric flowrate through the various bifurcating channels. Using a simplified circuit model, we justify the importance ensuring the hydrodynamic resistance of the main channel ( $R_m$ ) is much lower than that of the bifurcating channels.

**S4: Calibration of focusing flows:** In this section, we outline and justify the design parameters used to determine the flowrate ratio between the particle and focusing flows. In this way, we ensure that sample particles interact with each available bifurcating channel.

**S5: Equivalent circuit model justification and core equations:** Here, we outline the core theory and equations used to develop the circuit models used in sections S2 and S3 of the supporting information.

**S6: Two-stage flow method for selection of individual particles for deformability analysis:** In this section, we present a schematic which demonstrates the two stage mechanism that allows for the selection of single particles within the single channel batch mode device, allowing for the individual measurement of a particles threshold bypass pressure

**S7: Islet isolation and limitations to islet purity after density-gradient (DG) separation**

**S8: Increasing threshold bypass pressure of islets suggests recovery of basement membrane**

**S9: Detailed procedure for angiogenesis assay**

\* Corresponding Author. Fax: +1-434-924-8818.

Email: nswami@virginia.edu

## S1: Multichannel Continuous Separation Device justification of design criteria

To achieve continuous deformability-based separation of acinar populations from islets, the multichannel continuous flow separation device of Fig. 2 must be calibrated to meet two key design criteria, in order to apply the same pressures that were shown to differentiate islet versus acinar populations in the single-channel batch mode device. These criteria are: (1): the pressure differential across particles at the respective constriction geometry must be roughly equivalent in both devices, as per Fig. S1a for particle within device of Fig. 1 versus Fig.S1b for particle within device of Fig. 2); (2): the degree of deformation necessary to bypass the respective constriction must be the same in both devices. The second criterion can easily be achieved by ensuring equal cross-sectional areas for the respective constriction geometries within both device-types (Fig. S1). In order to achieve the first design criterion, it is important to consider the degree of occlusion of sample particles trapped at the constriction or bifurcating daughter channel (Fig. 2). As was explored by *Kuo et al.*, the pressure drop over a particle occluding a pore is strongly dependent on the degree of occlusion [1]. For complete occlusion (i.e. clogs), the pressure exerted on the particle is equal to the pressure differential across the entire pore, since the clogging particle prevents all fluid flow through the pore, thereby leading to a strong build-up of pressure on one side of the particle.

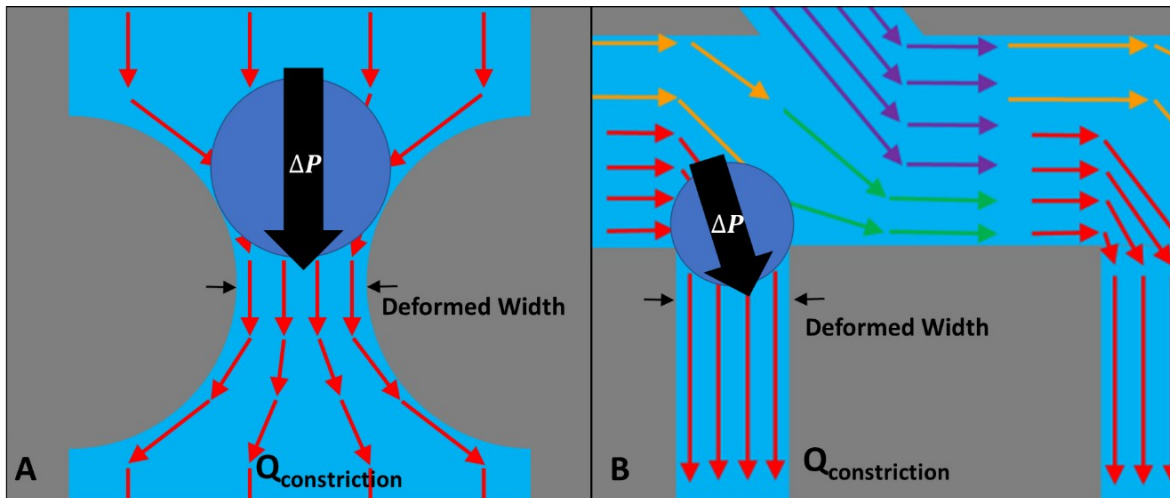


Figure S1 A: Schematic of the constriction geometry in the batch single channel threshold bypass pressure B: Schematic of the constriction geometry in the multi-channel continuous flow separation device. In order to maintain an equivalent pressure differential across sample particles, the cross sectional area of the channel and the volumetric flow rate through the channel correspond to those of the single channel device.

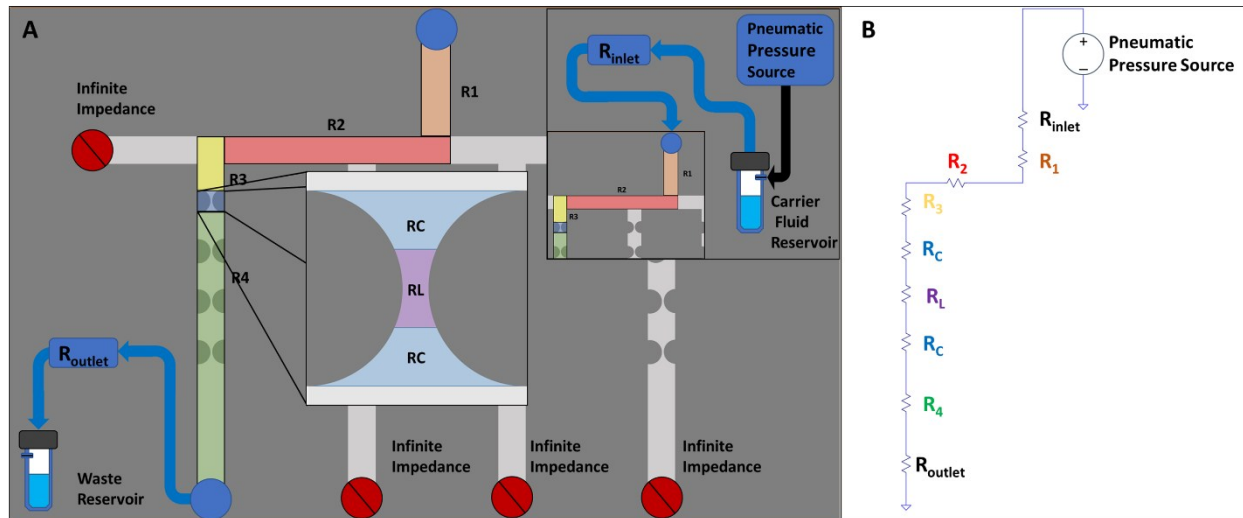
On the other hand, in cases of only partial occlusion, wherein the carrier fluid may still flow around the particle, far lower pressure differentials are achieved, with pressure primarily being exerted on the particle by drag forces from the carrier fluid. For cases of <75% occlusion, the pressure differentials rise only weakly with occlusion (within one or two orders of magnitude), following a similar relationship to the pressure imparted by a carrier fluid on an unobstructed particle.

$$\Delta P = \frac{3\mu v}{R} \dots Eq. (S1)$$

Where,  $\Delta P$  is the pressure differential across the particle,  $R$  is the radius of the particle, and  $v$  is the relative velocity of the carrier fluid. In this way, for two constrictions with identical cross sectional areas, the pressure applied to a particle will be equivalent, as long as the volumetric flowrate through both constrictions is the same (ensuring similar fluid velocity). For this reason, to match the pressure differential used to achieve deformation in the single channel batch measurement device (Fig. 1), the

multi-channel filtration device (Fig. 2) was designed such that the cross-sectional area of the bifurcating channels are similar to the constriction region of the single channel device. By matching the flow rates through these bifurcating channels to those within the single channel device the same pressure differentials may be achieved. By selecting a flowrate shown to primarily deform acinar tissue and not islets, isolation of the rigid islets was achieved.

## S2: Calculation of volumetric flowrate through threshold bypass pressure measurement device



In order to calibrate the flowrates used in the multichannel continuous flow separation device, it is

Figure S2: A: Schematic of the single channel threshold bypass pressure measurement device B: Hydraulic circuit model of A

necessary to determine the flowrate through the constriction geometries of the single channel batch mode device for each of the pressures applied during threshold bypass pressure measurement experiment. In order to do this, a hydrodynamic model of the single channel device was created. The layout and corresponding hydrodynamic circuit model of the device used for threshold bypass pressure measurement is depicted in figure S2A. Utilizing this model, the volumetric flowrate through the constriction geometry was calculated for varying pressure levels. The method outlined in section S5 of the supporting information were used to calculate the hydraulic resistance values for the constriction geometry (equation S7 and S8), the tubing inserted at the inlet and outlet of the device equation (equation S5), and the channels leading to and from the constrictions (equation S6). Since a pneumatic pressure source was used to apply a constant pressure differential across the device it was modeled as a voltage source. During device operation, a range of pressures from 25 to 500 mbar were applied at the device inlet. The corresponding applied pressures and volumetric flowrates through the device are provided in figure S3. The flowrates calculated from this analysis were then used to achieve separation in the filtration device.

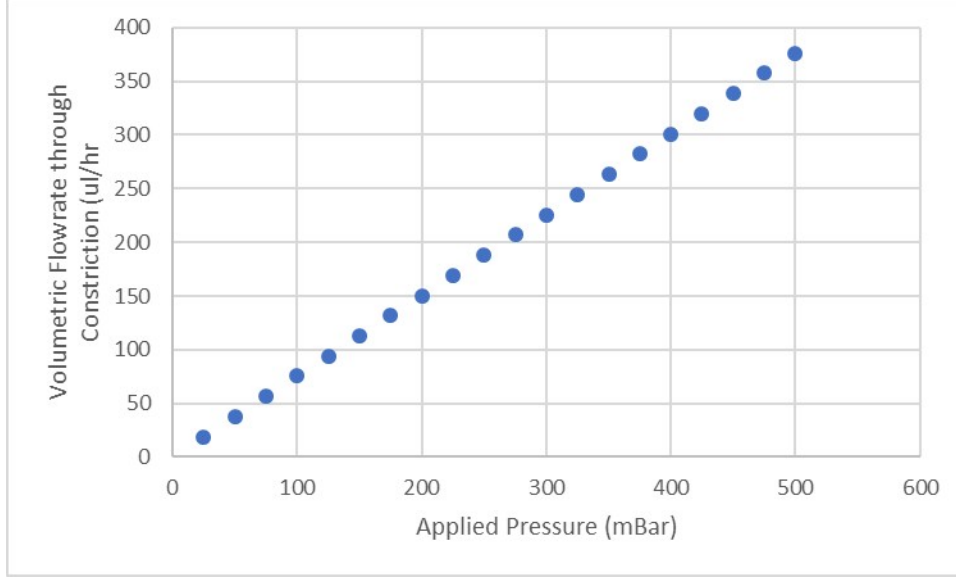


Figure S3: Volumetric flowrate through the single channel device versus the experimentally measured applied pressure.

### S3: Separation Device bifurcating channel optimization;

An array of parallel bifurcating constriction channels were used in the separation device to allow for the sequential trapping of multiple islets at each bifurcating point, prior to their removal during the collection mode. In order to maintain consistent and uniform flowrates through each bifurcating channel along the entire length of the main channel, a circuit model is used to optimize device design. As outlined in section S2 of the supporting information, the cross-sectional area of each bifurcating channel and the volumetric flowrate through each bifurcating channel (Fig. 2) was set to match that of the single constriction in the batch measurement device (Fig. 1). As such maintaining a relatively similar flowrate through each bifurcating channel independent of its position along the main channel is important to achieve a consistent pressure drop across trapped particles throughout the separation device. The layout and hydrodynamic circuit model for an N4 (i.e. a device having 4 bifurcating channels each preceded by a focusing flow) is depicted in figure S4 a and b. The hydrodynamic resistances of each component were determined using equation s3 from section 5 of the supporting information. The two independent pumping sources were constant flow rate syringe pumps and therefore modeled using current sources. In order to maintain a similar flowrate through each channel, the hydrodynamic resistance of each bifurcating channel must be designed to be several orders of magnitude higher than that of the main channel. This may be understood using a simplified version of the circuit for two bifurcating channels as depicted by the schematic in figure S4c and circuit model depicted in figure S4d. Here the two focusing flows and the fluid flow from upstream of the device are represented by individual current sources. The flowrate through the bifurcating channels will correlate to the current through the  $R_{\text{bifurcating}}$  resistors. Using super position in conjunction with the current divider equation the difference in flowrate between the first and second bifurcating channel may be written as follows.

$$\Delta Q_{1-2} = \frac{2R_m(Q_{ds} + Q_f)}{(2R_b + 2R_m)} \dots \text{Eq. (S2)}$$

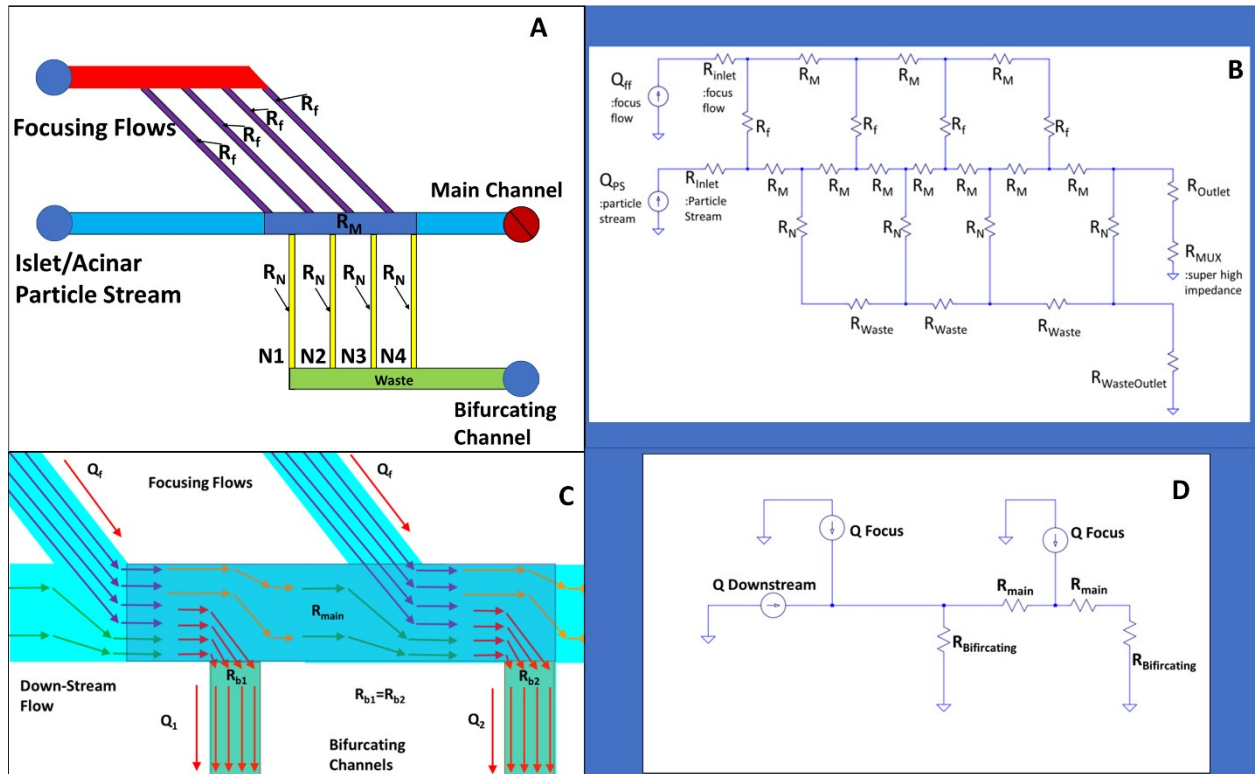


Figure S4: A schematic of an N4 (4 bifurcating channels) continuous flow separation device B: Hydraulic circuit model of the N4 device pictured in A. C: a simplified schematic of a 2N device. D: simplified Hydraulic circuit

Where,  $R_m$  is the hydrodynamic resistance of the main channel components,  $R_b$  is the hydrodynamic resistance of the bifurcating channels,  $Q_{ds}$  is the down-stream flowrate, and  $Q_f$  is the focusing flow-rate. This shows that the difference between the flowrates of these two channels may be limited by ensuring the hydrodynamic resistance of the main channel ( $R_m$ ) is much lower than that of the bifurcating channels. As equation S6 demonstrates this may be done by changing the channel geometries. In this case, as the width and height of the channels is determined by the application, the length of the channels has been increased. In this way variation of the bifurcating channel flowrates was limited to less than 1.2% for N 4 device depicted in figure S4 A.

## S4: Focusing Flows

For this application, the goal of the continuous flow separation device is to isolate and collect larger and less deformable particles (pancreatic islets) while removing smaller more deformable particles (acini tissue) to a waste port. As such, unlike in cases where the smaller or more deformable particles are the sample of value, in order to achieve a high purity final sample it is vital that all injected material interact with a bifurcating channel. In order to ensure this, focusing flows prior to each bifurcating channel are required to ensure all material introduced by the particle stream will interact with the first available free (with no trapped particle) channel. When fluid flow through a channel interacts with a bifurcating channel the flow is split between the main channel and the bifurcating channel as is described by the current divider equation. In cases where the fluid flow through these channels is laminar the width of fluid removed down the bifurcating channel is related to ratio of the flowrate through the main channel and the

bifurcation channel as is demonstrated in figure S5. Using a rough 2 dimensional model this width may be approximated as:

$$\frac{Q_2}{Q_1 + Q_2} = \frac{W_{ps}}{W_{tot}} : \frac{Q_4}{Q_3 + Q_4} = \frac{W_s}{W_{tot}} \dots Eq. (S3)$$

Where  $Q_1$  is the flowrate of the focusing flow,  $Q_2$  is the flowrate of the particle stream,  $Q_3$  is the flowrate through the main channel after the bifurcating channel,  $Q_4$  is the flowrate down the bifurcating channel,  $W_{ps}$  is the focused width due to the focusing flow,  $W_s$  is the selection width of the bifurcating channel, and  $W_{tot}$  is the total width of the channel.[2]

As particles carried by laminar flow tend to remain in the flow stream incident to their center of gravity, only particles whose center of gravity is within the width of removed fluid will interact with the bifurcating channel. For typical separation devices utilizing many bifurcating channels branching from the same main channel the decrease in flowrate along the main channel results in substantial variation in this selection width. Depending on a particles position within the width of the carrier stream this limits the selection points it may interact with, potentially leading to sample loss in cases where all available bifurcating channels have been filled by trapped low deformability particles. In order to allow all particles to interact with any of the bifurcating channels focusing flows prior to each bifurcating channel are used. This both focuses the particle stream and helps to maintain more consistent selection widths throughout the length of the device. For an N 4 device, in order to maintain a selection width of at least 200 um (50% of the main channel and 100% of the particle stream) the ratio of the flowrates delivered by the pumping mechanism driving the particle flow and the focusing flow is 1/2.1949. The width of the particle flow after focusing and the selection width for each bifurcating channel is given in table S1.

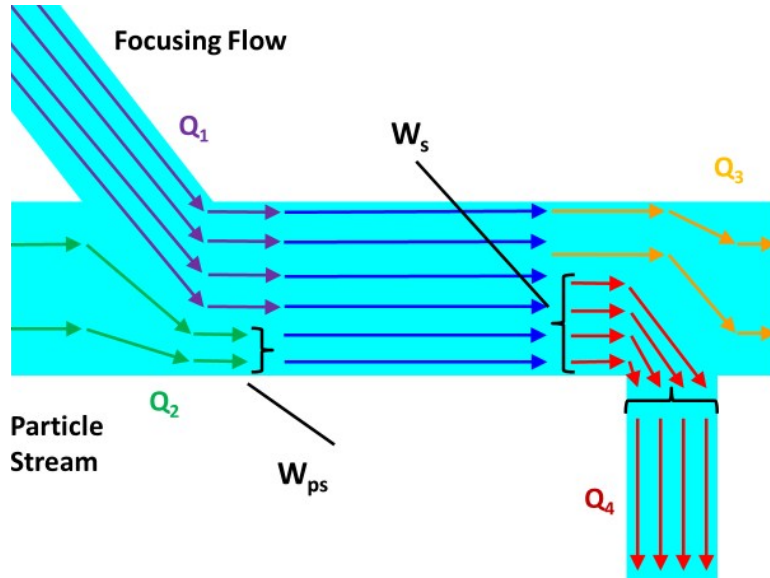


Figure S5: Particles carried by the carrier fluid will be focused to a position within the particle stream width ( $W_{ps}$ ) as determined by the ratio of the volumetric flowrate  $Q_1$  versus  $Q_2$ . Particles within the selection width ( $W_s$ ) will interact with the bifurcating channel as determined by the ratio of  $Q_3$  to  $Q_4$ . By ensuring  $W_{ps} < W_s$  all particles within the main channel will interact with the bifurcating channel.

N	$W_{ps}$ (um)	$W_s$ (um)
1	228.5714	226.2181
2	201.8138	262.758
3	163.6774	316.0964
4	104.5731	400

Table S1: Width of particle stream versus selection width for each bifurcating channel of an N 4 device

## S5: Linear Circuit Analogy and Equations

In order to achieve the first design criteria outlined above, hydraulic circuit models of both the batch measurement device and the continuous flow separation device were used to optimize their channel layout. The use of an electrical circuit analogy to model fluid flow through microfluidic devices has been well demonstrated and has proved a valuable tool for the design of microfluidic devices [2]. As is outlined by Hagen-Poiseuille's law, the volumetric flow rate of an incompressible liquid in laminar flow through a microfluidic channel is linearly proportional to the pressure differential over the channel length. This is analogous to the behavior of electrical current through a resistor as outlined by ohms law:

$$V = IR; \Delta p = QR_h \dots Eq. (S4)$$

Here, the volumetric flow rate ( $Q$ ) corresponds to current ( $I$ ), the pressure differential ( $\Delta p$ ) corresponds to voltage ( $V$ ), and the hydrodynamic resistance ( $R_h$ ) corresponds to the electrical resistance ( $R$ ). [2] Utilizing this analogy, standard electrical circuit analysis methods may be used to model fluid flow through a microfluidic device. In order to utilize this analogy, the various components of a microfluidic device must be represented as standard circuit elements, with pumping sources represented as either voltage (constant pressure sources such as pneumatic or vacuum sources) or current (constant flow rate sources such as syringe pumps) sources, whereas tubing, reservoirs, microfluidic channels and other structures are represented as resistor elements. For a straight length of tubing or channel with a constant circular cross section, the hydrodynamic resistance is described as follows

$$R_h = \frac{\Delta p \pi r^4}{8 \mu l} \dots Eq. (S5)$$

Where  $r$  is the radius of the circular cross section,  $\mu$  is the viscosity of the liquid, and  $l$  is the length of the tubing. [2] However, due to the planar nature of standard fabrication methods the cross sections of most microfluidic structures are not circular, with most having either a square or rectangular cross section. The hydraulic resistance of a rectangular channel may be approximated as follows

$$R_h = \frac{12 \mu l}{h^3 w (1 - .63 \frac{h}{w})} \dots Eq. (S6)$$

In cases when  $h < w$ , where  $h$  is the channel height and  $w$  is the channel width. [2] For a structures where the width of the channel varies along the length such as at constriction the hydrodynamic resistance may be given as

$$R_h = \frac{12 \eta}{h^3} \int_0^l \frac{1}{w(x) (1 - .63 \frac{h}{w(x)})} \dots Eq. (S7)$$

In cases when  $h < w$  and

$$R_h = \frac{12 \eta}{h} \int_0^l \frac{1}{w(x)^3 (1 - .63 \frac{w(x)}{h})} \dots Eq. (S8)$$

In cases when  $h > w$  where  $w(x)$  is a function which describes the channel width as a function of length.

**S6: Two-stage batch flow method for selection of individual sample particles**

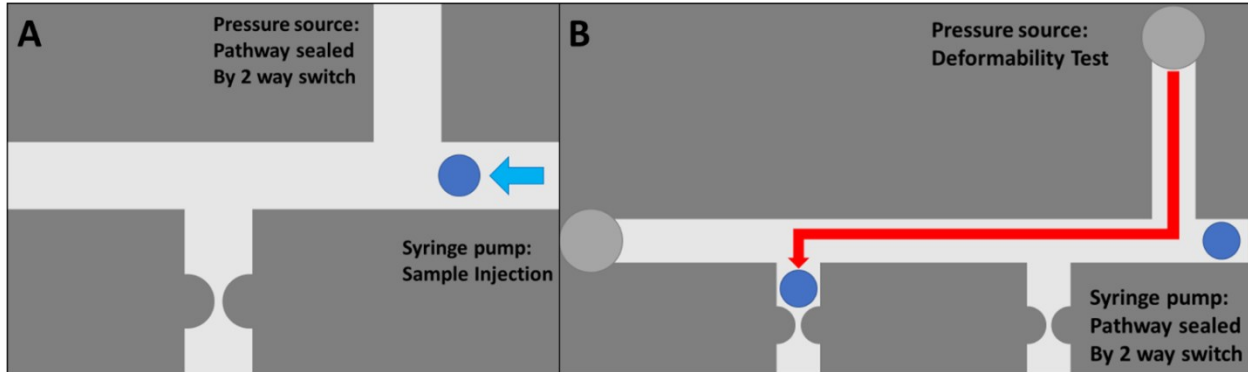


Figure S6: (A) syringe pump is used to inject sample delivering a particles to the inverted T-junction; (B) individual particles driven under pressure flow towards constriction of interest.

**S7: Limitations on islet purity after density gradient separation:**

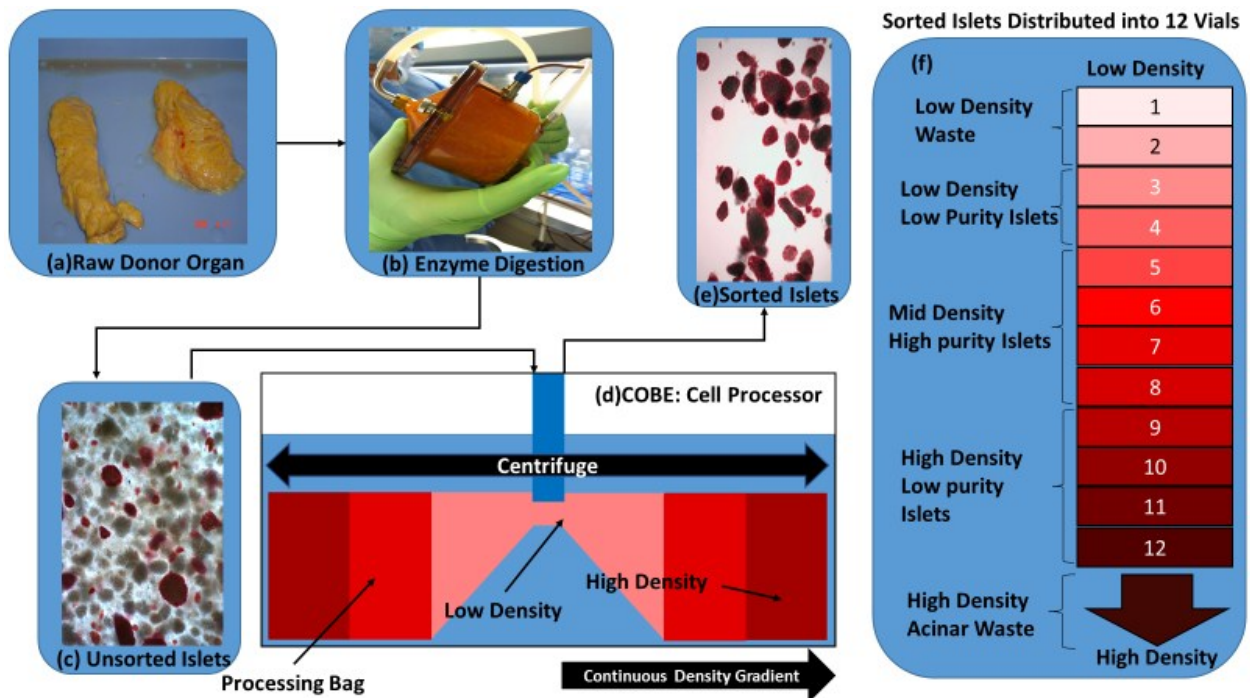


Figure S7: Schematic of the sample preparation process: (a) raw donor organs; (b) enzyme digestion; (c) sample mixture of islets (stained for insulin) and acinar tissue; (d) COBE cell processor for density based separation; (e) sorted islets from a mixture of samples from centrifuged fractions (f).

The limitations on % purity of the islet samples generated by the density gradient (DG) method (**Fig. S7**) were explored based on 22 islet isolation procedures on human donor research organs. Based on estimated purity levels, the packed tissue volume of islets and acinar aggregates within each of the 12 fractions collected from the COBE system for DG separation is plotted in **Fig. S8a**. It is noteworthy that the acinar tissue populations are predominantly trapped within the higher density media, thereby appearing primarily in the #9-12 COBE fractions, while the islets are broadly distributed over the central centrifuged fractions: #3-8 from COBE system. As is typically done prior to incubation, the islet containing fractions were combined into four bins, based on the sample purity levels (i.e. % islets): high purity (>80%), medium purity (80%-50%), low purity (50%-30%) and waste (<30 %) samples. Within these four bins, **Fig. S8b** shows the distribution of islet volume (estimated from the purity and packed tissue volume of the combined fraction), while **Fig. S8c** shows the total packed tissue volume after each isolation step. Based on this, it is apparent that while the islet volume remains relatively constant across the low, medium and high purity sample bins (each representing ~28% of the overall islet yield from donor organs), the total packed tissue volume within these bins drops with increasing islet purity levels, thereby indicating that the transplant plug cannot be generated solely from a single sample bin, due to the insufficient islet numbers within the high purity sample bin. Currently, islet transplant samples must meet the following criteria: (i) the total number of islets must be greater than 5,000 for every kg of the recipients body weight; (ii) viable islets must form 30% of the transplant plug, with a viable islet defined as those with at least 70% of component cells lacking the propidium iodide (PI) stain; and (iii) the total transplant must be below 10 mL of packed tissue. Since islet yield from the two starting donor organs is relatively evenly distributed across the low, medium and high purity sample bins, the bins must be combined to form a transplant plug of less than 10 mL packed tissue volume. Based on this, from sixteen donor research organs used in the current investigation, we combined the isolated islet samples from high, medium, and low purity bins to form eight potential transplant plugs. The average purity of the transplant plug produced by this method was found to be around 60%, with none of the transplants exceeding 72% and the average packed tissue volume of the plug was around 5.55 mL, with none exceeding 8.5 mL. Due to the inability of the sample bins generated by the density gradient separation method to reach higher purity levels, we infer that there is a significant level of density overlap between the pancreatic islets and a significant quantity of the acinar tissue. Hence, while the DG separation method is able to remove a majority of the acinar tissue aggregates, the generated transplant plug contains ~40% acinar tissue aggregates, due to large acinar levels within the pre-purification slurry[3] and the wide distribution of islets across the collected sample bins, thereby leading to a transplant plug with relatively low purity. While this plug meets the current transplant requirements, it is likely that the high volume of acinar tissue within the transplant plug exacerbates the autoimmune response, resulting in an increased likelihood of transplant rejection[3],[4]. Furthermore, the waste sample bin (i.e. those with <30% purity) of high volume that is usually discarded causes a 15% loss in the overall islets from the donor organ, representing an 85% collection efficiency. Finally, within about 20% of the DG separation cases investigated for this

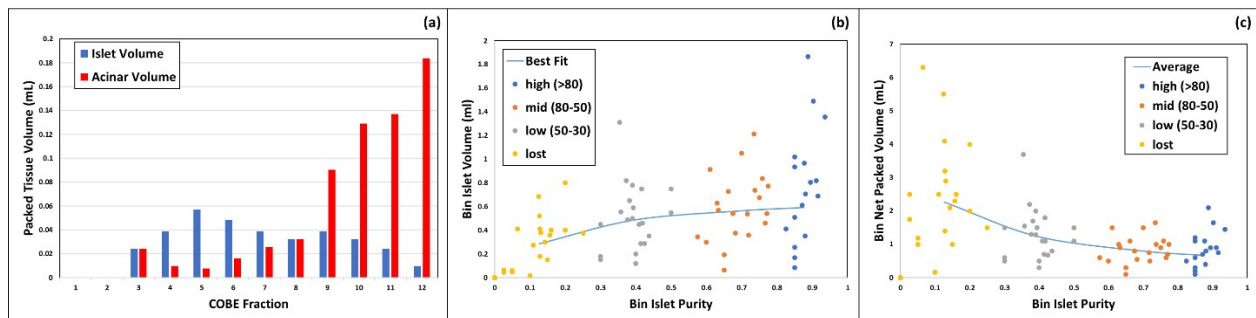
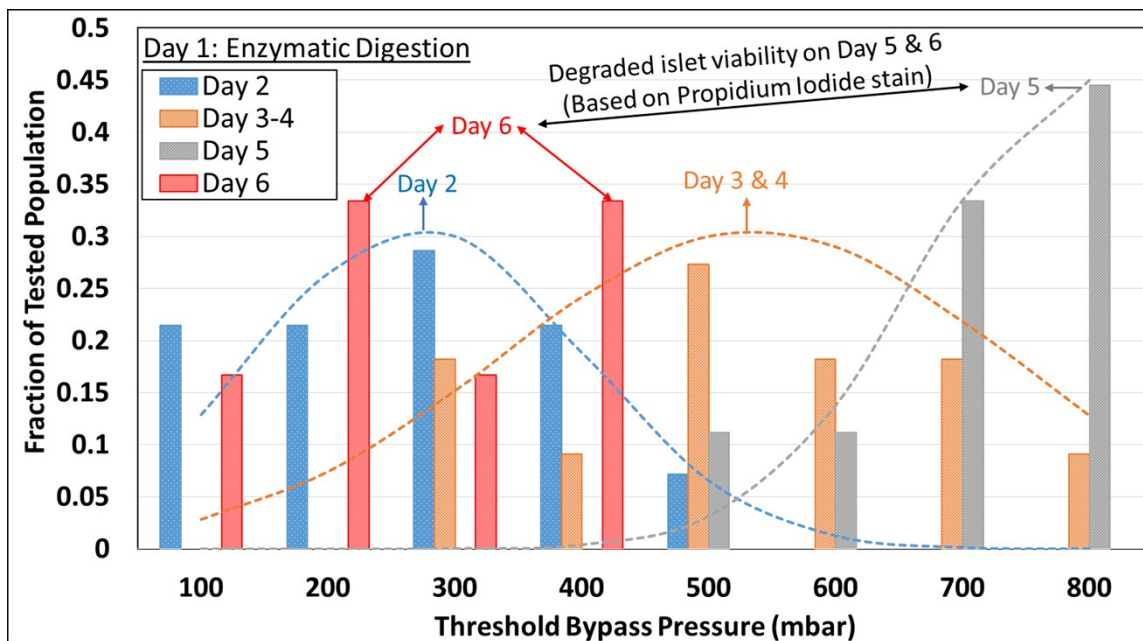


Figure S8: (a) Packed tissue volume (mL) of islets versus acinar within each of the centrifuged fractions from COBE system; (b) packed tissue volume for islets and (c) Total packed tissue volume within the bins characterized as: high purity (blue: > 80%), medium purity (orange: 50-80%), low purity (grey: 30-50%) and waste samples (yellow: < 30% purity).

study, the method failed to produce a high purity sample bin (>80% islets), suggesting a great degree of variability in the isolated fractions. Hence, we investigate microfluidic deformability-based separation to enhance the islet purity

**S8: Increasing threshold bypass pressure of islets suggests recovery of basement membrane:**

Following digestion of pancreas on Day 1, the threshold bypass pressure of digested islets in Fig S9 measured onward from Day 2 shows a successive increase up to Day 5, followed by gradual loss of islet viability. The threshold bypass pressure for acinar tissue remains relatively unchanged, as per Fig. 5b of manuscript. This strongly suggests regrowth of the damaged basement membrane of the islets in the 24-48 hour period after enzymatic digestion of the pancreas, thereby causing islets to become more rigid versus acinar populations. The continuing role of extracellular matrix (ECM) is further substantiated by the uniformity in trend of islet stiffness, as measured by area of the respective multi-cell aggregate versus its threshold bypass pressure, whereas acinar tissues show a heterogeneous deformability stiffness distribution that is likely due to their degraded ECM. Hence, the samples within this work are standardized to those obtained after the 24-48 hour period (just after Day 2) wherein islets retain their highest % viability and are significantly more rigid than acinar populations.



**Fig. S9:** Following enzymatic digestion of pancreas on Day 1, the islet populations show a gradual increase in rigidity that is likely due to regrowth of their damaged basement membrane, until the loss of islet viability after Day 5. On the other hand, the threshold bypass pressure of the acinar tissue populations remains unchanged.

**S9 – Detailed procedure of angiogenesis assay to measure vascularization of transplanted islets:**

Mice were anesthetized with an intraperitoneal injection of ketamine/xylazine/atropine (60/4/0.2 mg/kg body weight) (Zoetis; Kalamazoo, MI / West-Ward; Eatontown, NJ / Lloyd Laboratories; Shenandoah, IA), and a drop of sterile 0.5% Proparacaine Hydrochloride Ophthalmic solution (Henry Schein Inc; Melville, NY) was added as a topical anesthetic to numb the eye before treatment. A small incision was placed about 1 mm away from the capillary network surrounding the cornea, parallel to the capillary vessels. Using a sterile surgical blade, an incision was then made in the cornea to make a small pocket between the corneal epithelial layers, toward the capillary network. This was done carefully, so as to not

rupture the cornea or poke through to the anterior chamber of the eye. Using a 10  $\mu$ L pipette tip, islets were then transferred from warm and sterile PBS onto the surface of the cornea, just outside the micropocket. The islets were then slid very gently into the micropocket using either a 27-gauge needle or jeweler's forceps. Finally, the micropocket was lightly closed using jeweler's forceps to prevent the islets from regurgitating out of the cornea pocket. Seven days after transplantation, bright field images of corneas under 4X magnification were obtained using a Nikon Digital Sight DS-L2 Camera Controller (Nikon Instruments Inc, Melville, NY; Model 214602) to observe viability of the islets in the cornea micropocket. To harvest tissues for further analysis, anesthetized mice were euthanized in a CO<sub>2</sub> chamber and secondarily euthanized with a cervical spine dislocation. Corneas were harvested immediately, then fixed and permeabilized in 100% acetone for 25 minutes at room temperature. Next, the tissues were blocked with 5% normal mouse serum and 2% bovine serum albumin in phosphate buffered saline (PBS). To visualize blood vessels, corneas were superfused with the endothelial cell marker, rat monoclonal anti-mouse cluster of differentiation 31 (CD31) (Dianova; Hamburg, Germany; 1:250 dilution), washed eight times for five minutes in 0.1% saponin in PBS, and superfused again with goat anti-rat IgG (H+L) FITC (abcam; Cambridge, UK; 1:400 dilution). Corneas with transplanted islets were whole-mounted with coverslips on gelatin-coated slides using a 50:50 glycerol/PBS solution. Digital images of the corneal and islet vasculature were acquired using confocal microscopy (Nikon Instruments Incorporated, Melville, NY; Model TE200-E2; 10X, 20X, and 60X objectives); full-thickness z-stack (2  $\mu$ m steps) volume renders were used to capture the entire thickness of the corneal and islet vascular networks in each field of view.

## References

- [1] J. S. Kuo, Y. X. Zhao, P. G. Schiro, L. Y. Ng, D. S. W. Lim, J. P. Shelby, *et al.*, "Deformability considerations in filtration of biological cells," *Lab on a Chip*, vol. 10, pp. 837-842, 2010.
- [2] K. W. Oh, K. Lee, B. Ahn, and E. P. Furlani, "Design of pressure-driven microfluidic networks using electric circuit analogy," *Lab on a Chip*, vol. 12, pp. 515-545, 2012.
- [3] H. Ichii, A. Pileggi, R. D. Molano, D. A. Baidal, A. Khan, Y. Kuroda, *et al.*, "Rescue purification maximizes the use of human islet preparations for transplantation," *American Journal of Transplantation*, vol. 5, pp. 21-30, Jan 2005.
- [4] D. W. R. Gray, R. Sutton, P. Mcshane, M. Peters, and P. J. Morris, "Exocrine Contamination Impairs Implantation of Pancreatic-Islets Transplanted beneath the Kidney Capsule," *Journal of Surgical Research*, vol. 45, pp. 432-442, Nov 1988.